Noncollinear ferrimagnetic ground state in $Ni(NO_3)_2$

O. S. Volkova,[1,2] V. V. Mazurenko,[2] I. V. Solovyev,[2,3] E. B. Deeva,[4] I. V. Morozov,[4] J.-Y. Lin,[5] C. K. Wen,[5] J. M. Chen,[6] M. Abdel-Hafiez,[7,8] and A. N. Vasiliev[1,2,9]

[1]*Low Temperature Physics and Superconductivity Department, Physics Faculty, M.V. Lomonosov Moscow State University, Moscow 119991, Russia*

[2]*Theoretical Physics and Applied Mathematics Department, Institute of Physics and Technology, Ural Federal University, Ekaterinburg 620002, Russia*

[3]*National Institute for Materials Science, 1-2-1 Sengen, Tsukuba, Ibaraki 305-0047, Japan*

[4]*Inorganic Chemistry Department, Chemistry Faculty, M.V. Lomonosov Moscow State University, Moscow 119991, Russia*

[5]*Physics Department, National Chiao-Tung University, Hsinchu 30076, Taiwan*

[6]*National Synchrotron Radiation Research Center, Hsinchu 30076, Taiwan*

[7]*Center for High Pressure Science and Technology Advanced Research, 1690 Cailun Road, Shanghai 201203, China*

[8]*Physics Department, Faculty of Science, Fayoum University, 63514 Fayoum, Egypt*

[9]*National University of Science and Technology "MISiS," Moscow 119049, Russia*

(Received 26 January 2014; revised manuscript received 16 August 2014; published 10 October 2014)

Both spin-liquid and magnetically ordered phases of both half-integer and integer low-spin quantum magnets are of interest, since the magnetic structures found in the latter case usually have no classical counterparts. Such a magnetic structure was found in a combined experimental and theoretical study of the integer spin system $Ni(NO_3)_2$. Our thermodynamic measurements have revealed a magnetically ordered phase with small spontaneous magnetization at $T_C = 5.5$ K. The magnetization saturation of about $2\mu_B$ at low temperatures corresponds to the high-spin state ($S = 1$) of Ni^{2+} ions evidenced in $L_{2,3}$ edges in x-ray absorption spectroscopy spectra. We show that a consistent description of the available data is possible within a noncollinear umbrella-type ferrimagnetic ground state model for which both intra- and interlayer magnetic interactions should be antiferromagnetic. Such a scenario is suggested by the first-principles and model calculations.

DOI: 10.1103/PhysRevB.90.134407 PACS number(s): 75.25.−j, 71.20.−b, 75.30.Et, 75.50.Gg

I. INTRODUCTION

The attractiveness of antiferromagnetic kagomé lattices is supported by a unique triangular motif in a two-dimensional arrangement of magnetic ions. For the spin-1/2 case, numerous treatments point to a disordered spin-liquid ground state with an appreciably small spin gap compared with the exchange parameter [1–3].The significantly less studied spin-1 kagomé lattices are assumed to possess the hexagonal singlet solid state [4–6]. Experimental studies of spin-1 kagomé lattices revealed either the absence of long-range order [7,8] or an antiferromagnetic/glassy state [9–14] typical in systems with competing exchange interactions. On the other hand, the existence of ferromagnetism in kagomé compounds has been intensively discussed *theoretically*, albeit with the presence of antiferromagnetic exchange. The kinetic origin of ferromagnetism for a partially filled kagomé lattice was discussed [15]. The dipolar interactions were shown to support the nonuniform ferromagnetic state in kagomé lattices [16]. Besides, large single-ion anisotropy compared with exchange interaction might inspire the xy ferromagnetic state into spin-1 kagomé antiferromagnets [17]. The entropy gain due to the phase transition into a magneto-ordered state, with spontaneous moment in finite "weathervane loops" separated in kagomé spin-1 anisotropic antiferromagnetic lattices, was also discussed [18]. Here, we suggest a noncollinear ferrimagnetic ground state model for $Ni(NO_3)_2$, where both intra- and interlayer magnetic interactions are assumed to be antiferromagnetic.

II. EXPERIMENTAL

While the hydrates of the transition metal nitrates constitute a vast and well-documented family of compounds, e.g., $Cu(NO_3)_2 \times nH_2O$ with $n = 1$, 2.5, 6 [19–22] or $Ni(NO_3)_2 \times mH_2O$ with $m = 2$, 4, 6 [23], information on the physical properties of the anhydrous nitrates of transition metals is very limited and restricted to infrared spectra [24] and electronic structure, as obtained from low-energy photoelectron spectroscopy [25]. Mainly, this is because these forms are quite hygroscopic and, as a consequence, difficult to handle. At the same time, the apparent simplicity of the chemical formula and intriguing motifs in the transition metal arrangement require study in this uncharted territory.

The nickel (II) nitrate, $Ni(NO_3)_2$, crystallizes in a rhombohedral $R\bar{3}$ space group ($a = 10.332(1)$ Å, $c = 12.658(2)$ Å, $Z = 12$) with two nonequivalent positions for Ni^{2+} ions in the ratio Ni(1):Ni(2) = 3:1 [25]. As shown in Fig. 1, the NiO_6 octahedra share all corners with the NO_3 groups to form the framework structure. In the ab plane, the Ni(1) ions linked through regular $N(1)O_3$ triangles form structurally perfect kagomé layers with Ni(2) ions occupying the hexagons. Within this plane, the Ni(2) ions are linked to Ni(1) ions through nonsymmetrical isosceles $N(2)O_3$ units. The same $N(2)O_3$ nitrate groups link successive layers along the c axis. With respect to this axis, the successive layers are shifted by quarter periods along the a and b axes.

The polycrystalline samples of $Ni(NO_3)_2$ were prepared by crystallization from a nitric acid solution in the presence

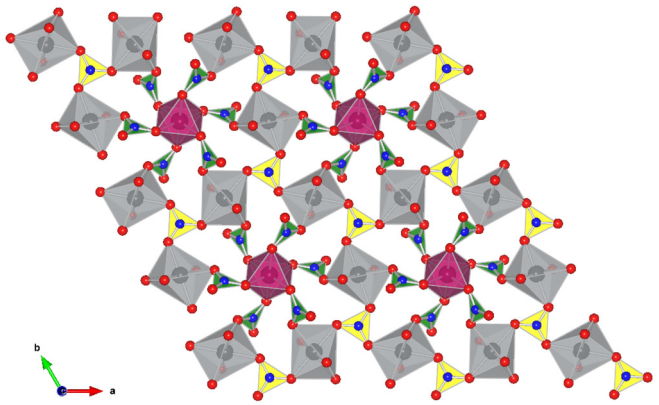

FIG. 1. (Color online) The crystal structure of $Ni(NO_3)_2$ in the *ab* plane. The Ni(1) and Ni(2) ions are shown in a gray and purple octahedral oxygen environment. The regular and isosceles nitrate groups are shown by yellow and green triangles. The Ni(1) forms kagomé-type layers, while Ni(2) ions occupy the hexagonal cavities.

of an adsorbent-desiccant [26]. Thermodynamic properties were measured by a Physical Property Measurement System (PPMS)-9T (Quantum Design) with the sample mounting done in the nitrogen atmosphere. The x-ray absorption spectroscopy (XAS) experiments were performed at the H-SGM beamline at the National Synchrotron Radiation Research Center in Taiwan. X-ray absorption spectroscopy was recorded in total electron yield in an ultrahigh vacuum ($\sim 10^{-10}$ mbar) chamber.

A simple monochrome picture of a three-dimensional triangular lattice in $Ni(NO_3)_2$ consisting of Ni^{2+} ions linked by $(NO_3)^{-1}$ groups transforms into a layered, "filled" kagomé network if the nonequivalent positions of nickel in octahedral surroundings are rendered in different colors and the regular and isosceles nitrate triangles are distinguished, as shown in Fig. 1. In the case of *ferromagnetic* coupling between magnetic species, there is no difference between black-and-white and in-color representations. The colors are of key importance, however, when *antiferromagnetic* coupling prevails in the system. Experimental observation of "simple" ferromagnetism in $Ni(NO_3)_2$ appeared to be in sharp disagreement with the first-principles and model calculations, revealing the dominance of antiferromagnetic exchange interactions.

III. THERMODYNAMICS

The temperature dependence of dc magnetic susceptibility, $\chi = M/B$ taken at $B = 0.1$ T in $Ni(NO_3)_2$, is shown in Fig. 2. At high temperatures, the magnetic susceptibility follows the Curie-Weiss law with the addition of the temperature independent term $\chi = \chi_0 + C/(T - \Theta)$, where $\chi_0 = 2.3 \times 10^{-4}$ emu/mol, Curie constant $C = 1.3$ K emu/mol, and negligibly small Weiss temperature Θ is about ± 1 K. The value of the temperature independent term corresponds to the summation of negative Pascal's constants of Ni^{2+} ions and $(NO_3)^-$ groups $\chi_{dia} = -0.5 \times 10^{-4}$ emu/mol [27] and a positive Van Vleck term of Ni^{2+} ions $\chi = 2.8 \times 10^{-4}$ emu/mol [28]. At cooling, the $\chi(T)$ dependence sharply deviates upward, signaling the formation of a magnetically ordered state in the system. At low temperatures, the hysteretic behavior of magnetization,

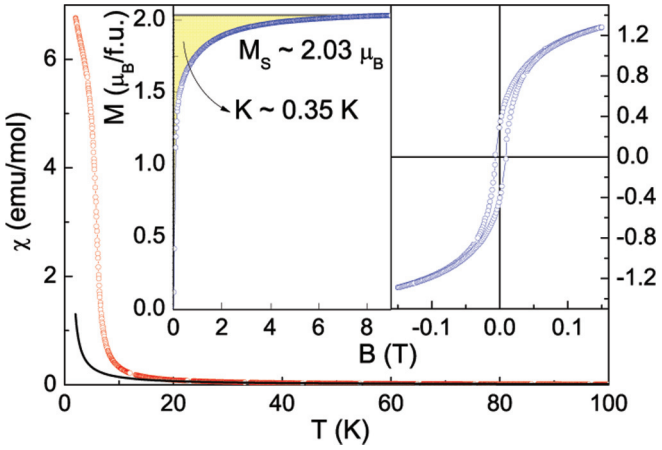

FIG. 2. (Color online) The temperature dependence of magnetic susceptibility in $Ni(NO_3)_2$ taken at $B = 0.1$ T (symbols), the solid line represents the high-temperature fit of experimental data. The field dependence of magnetization and the hysteresis loop taken at $T = 2$ K are shown in the left and right insets, respectively.

shown in the right inset of Fig. 2, is that of a soft magnet with the remanent magnetization $0.3\mu_B$, a coercive force $B_C = 5.4$ kA/m, and the saturation magnetization $M_S \sim 2\mu_B$ at 2 K, as shown in the left inset of Fig. 2. The area under the magnetization curve taken at the lowest temperature 2 K allows estimating the upper limit of magnetocrystalline anisotropy K in $Ni(NO_3)_2$ as about 0.35 K ($\sim$0.03 meV). To define the exact value of the magnetic ordering temperature, the magnetization curves were measured at several fixed temperatures in steps of 0.25 K. The results plotted as B/M vs. M^2 indicate that $Ni(NO_3)_2$ orders magnetically at $T_C = 5.5$ K $\pm$ 0.25 K, as shown in the right panel of Fig. 3.

Further evidence for the phase transition into a magnetically ordered state was obtained at specific heat measurements. As shown in the left panel of Fig. 3, the C_p vs. T curve demonstrates a sharp λ-type anomaly at $T_C = 5.5$ K, which indicates a second-order phase transition from a paramagnetic state to

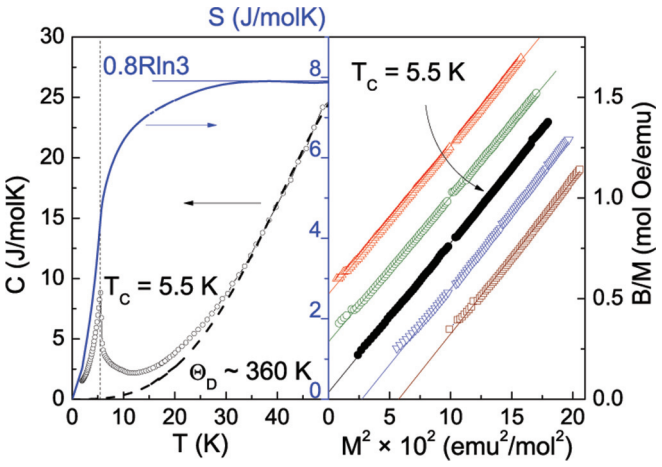

FIG. 3. (Color online) The temperature dependencies of specific heat (symbols) and magnetic entropy (solid line) in $Ni(NO_3)_2$. The dashed line represents the lattice contribution to the specific heat (left panel). The Arrott plot in $Ni(NO_3)_2$ (right panel).

magnetically ordered state. The magnetic entropy released below T_C amounts to $S_{mag} \sim 4.5$ J/mol K, which constitutes about one-half of the expected value ($R \ln 3$) for Ni^{2+} high-spin state $S = 1$. At $T \gg T_C$, the specific heat possesses only the lattice contribution that can be approximated by the cubic term $C_p = \beta T^3$ with $\beta = 3.75 \times 10^{-4}$ J/mol K^4. This value allows estimating the Debye temperature Θ_D in $Ni(NO_3)_2$ at about 360 K.

IV. X-RAY ABSORPTION SPECTROSCOPY

To study the spin state of nickel ions, the XAS at the nickel $L_{2,3}$ edge was employed for $Ni(NO_3)_2$ and a NiO as a reference. Two nickel sites in $Ni(NO_3)_2$ have slightly different NiO_6 octahedral environments. In the NiO_6 octahedra the Ni $3d$ degenerate state was separated into e_g and t_{2g} states with 10 Dq difference by the crystal field, and the e_g state was separated into x^2-y^2 and $3z^2$-r^2 states with Δe_g difference by the distortion. Depending on the ratio between Hund's coupling, J_H and Δe_g splitting, the Ni^{2+} ions ($3d^8$) may exhibit either low-spin (LS; $S = 0$) or high-spin (HS; $S = 1$) states. The oxygen octahedra surrounding Ni(1) and Ni(2) atoms in the $Ni(NO_3)_2$ compound are rather similar and slightly distorted. Such a distortion may lift the degeneracy of the e_g levels. The local symmetry of the Ni(1) atoms is somewhat lower. Therefore, the atomic e_g levels will slightly split. According to our first-principles calculations, this splitting is about 50 meV. On the other hand, the local symmetry of the Ni(2) atoms is higher. Therefore, the e_g levels will remain almost degenerate, forming a two-dimensional representation of the space group $R\bar{3}$. Thus, it is reasonable to expect that nickel ions in $Ni(NO_3)_2$ will form the high-spin state.

The Ni $L_{2,3}$ ($2p \rightarrow 3d$) absorption spectrum obeys the dipole selection rule: the transition can be described as $\alpha|2p^6 3d^n\rangle + \beta|2p^6 3d^{n+1}\underline{L}\rangle \rightarrow \alpha'|2p^5 3d^{n+1}\rangle + \beta'|2p^5 3d^n + 2\underline{L}\rangle$, where $\underline{L}$ denotes a charge transfer from ligand to nickel, α and β are the initial electronic states, and α' and β' are the final electronic states. The Ni $2p$ core-hole spin-orbit coupling splits the spectrum into two parts, namely the L_3 (853 eV) and L_2 (871 eV) white line regions. The line shape of the spectrum depends on the atomic multiplet effect, including Ni $3d$-$3d$ and $2p$-$3d$ Coulomb and exchange interactions, hybridization of the Ni $3d$ orbital with the O $2p$ ligands, and the local crystal field.

Figure 4 shows the Ni $L_{2,3}$ XAS experimental spectra of NiO and $Ni(NO_3)_2$ taken at room temperature. NiO is generally accepted to have divalent nickel with a HS ($S = 1$) state. In the Ni L_3 edge, both NiO and $Ni(NO_3)_2$ have a peak at 853.35 eV, which can be used to determine the valence of nickel ions [29]. The results indicate that the nickel ions are also divalent in $Ni(NO_3)_2$ [30,31]. The second peak at 855.1 eV of the L_3 edge in $Ni(NO_3)_2$ has a higher intensity than in NiO. There also exists a shoulder feature at 856.5 eV in the L_3 edge of NiO, while this feature is absent in that of $Ni(NO_3)_2$. These two differences come from the ligand field multiplet effect, which implies different Ni local structures in these two compounds. The L_2 edge of both $Ni(NO_3)_2$ and NiO_2 splits into two peaks. The L_2 edge of $Ni(NO_3)_2$ has a slightly lower intensity at 870.7 eV and a significantly higher intensity at 871.8 eV compared with those of NiO_2. The broad peak at

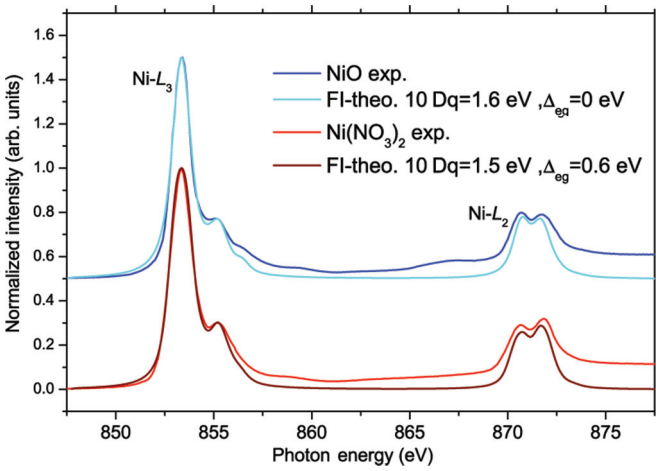

FIG. 4. (Color online) Nickel $L_{2,3}$ edge XAS data of NiO (dashed line) and $Ni(NO_3)_2$ (solid line) in total electron yield.

859 eV is the $|2p^6 3d^9\underline{L}\rangle \rightarrow |2p^5 3d^{10}\underline{L}\rangle$ transition from the charge transfer effect, while a broad feature at 866.7 eV in the NiO spectrum is the $2p \rightarrow 4s$-like transition, called a continued edge jump [29].

To confirm the spin state of divalent nickel in $Ni(NO_3)_2$, we discuss the theoretical calculations of the $L_{2,3}$ XAS line shape using the full atomic multiplet theory, together with hybridization of the Ni $3d$ orbital with the O $2p$ ligands and the point charge crystal field in the NiO_6 cluster [32]. For the NiO case, the NiO_6 octahedron is almost undistorted, and the nickel ion has the same Ni-O bond length with all six O neighbors. In the calculations, we used the hybridization coefficient $pd\sigma = -1.29$ eV [33], and set $\Delta e_g = 0$ eV (undistorted). The best fit for NiO spectra is with 10 Dq = 1.0 eV, consistent with the recent results of resonant inelastic x-ray scattering [34]. For the $Ni(NO_3)_2$ case, the crystal structure shows the average Ni-O bond length of 2.071 Å, very close to the bond length of 2.08(1) Å in NiO [35,36]. Since NiO and $Ni(NO_3)_2$ have nearly the same average Ni-O bond length, 10 Dq should also be close in both cases. Indeed, the calculations show10 Dq = 0.9 eV is the best fit for $Ni(NO_3)_2$. Therefore, the spin state of $Ni(NO_3)_2$ is still HS according to XAS.

V. FIRST-PRINCIPLES CALCULATIONS

The magnetic subsystem in $Ni(NO_3)_2$ can be considered either a two-dimensional or three-dimensional network depending on relative magnitudes of intralayer and interlayer exchange interaction parameters. Besides, the two-dimensional layers can be treated as either triangular or a kagomé type depending on the relative magnitudes of Ni(1)–Ni(1) and Ni(1)–Ni(2) exchange interaction parameters J_i. In this paper, these parameters were calculated using the magnetic force theorem [37,38] within a local spin density approximation (LSDA) [39,40], taking into account the onsite Coulomb interaction (LSDA + U) [41] and the Hartree-Fock (HF) approximation [42]. We used the known crystal structure data [25].

Before discussing magnetic couplings in the $Ni(NO_3)_2$ system, we focus on the ground state electronic and

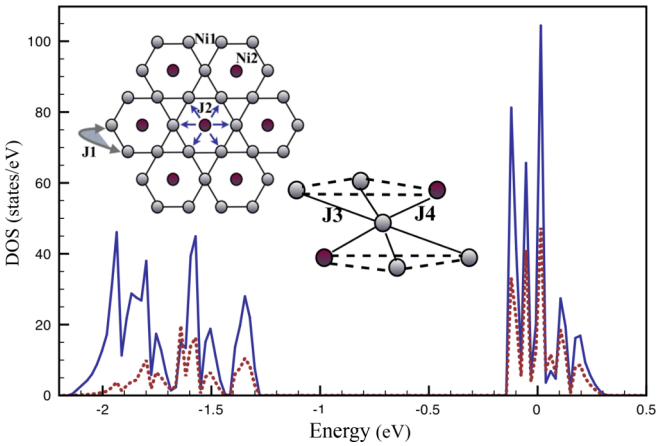

FIG. 5. (Color online) The $Ni(NO_3)_2$ partial densities of states (DOS) calculated by using LDA. The red dotted and blue solid curves correspond to O $2p$ and Ni $3d$ states. The insets: topology of intralayer and interlayer exchange interactions.

magnetic properties. As follows from the band structure local density approximation (LDA) calculations within the tight-binding linear muffin-tin orbital atomic sphere approximation method [39,40], shown in Fig. 5, there is strong hybridization of nickel and oxygen states. The fully occupied t_{2g} and half-filled e_g states are centered at -1.7 eV and 0 eV, respectively. The calculated value of 10 Dq $=$ 1.7 eV is to be compared with that found in XAS 10 Dq $=$ 1.0 eV. The difference is due to the charge transfer effect directly observed by resonant inelastic x-ray scattering [34], though in NiO.

To reproduce the insulating ground state of $Ni(NO_3)_2$ we employ the LSDA+U approach with onsite Coulomb and intra-atomic exchange interactions as 3 eV and 0.9 eV, respectively. Since the e_g band is half-filled, we observe only the splitting between fully occupied spin-up and empty spin-down states, as shown in Fig. 6. The account of the Coulomb interaction does not change the structure of the e_g band. It is due to the fact that both e_g orbitals are either occupied or empty. The energy gap of 1.46 eV opens between occupied (spin-up) and empty (spin-down) states. The calculated magnetic moments of nickel and the nearest oxygen atoms were found collinear

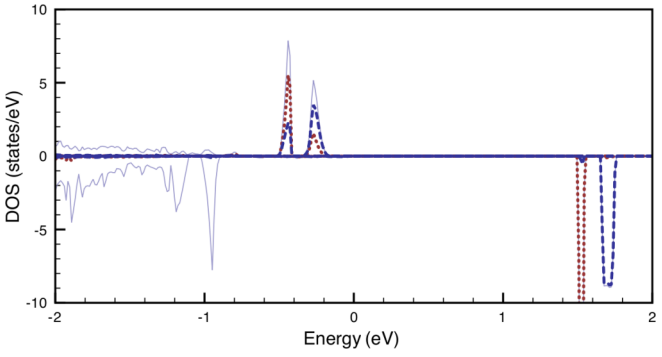

FIG. 6. (Color online) Total and partial DOS for Ni(1)-1 obtained from the LSDA $+$ U calculations. The gray, red dotted, and blue dashed lines correspond to total, $3z^2$-r^2, and x^2-y^2 states, respectively.

TABLE I. Isotropic exchange interaction parameters in $Ni(NO_3)_2$ obtained from LSDA, LSDA $+$ U, and HF calculations (meV). The corresponding interaction paths are shown in Fig. 5.

Exchange interaction	LSDA	LSDA $+$ U	HF
J_1	0.44	0.37	1.01
J_2	0.1	0.15	0.53
J_3	0.24	0.23	0.72
J_4	0.06	0.08	0.38

and equal to $1.45\mu_B$ and about $0.09\mu_B$, respectively. The obtained total magnetization of $Ni(NO_3)_2$ per formula unit is $2\mu_B$, in agreement with the experimentally estimated value.

For every superexchange interaction of nickel ions through nitrate groups, the estimations using the magnetic force theorem [37,38] provided a positive (antiferromagnetic) sign with magnitudes given in Table I. The largest exchange interaction parameters, $J_1 = 5.1$ K and $J_3 = 2.8$ K, correspond to intralayer and interlayer Ni(1)–Ni(1) (5.16 Å) interactions, respectively. The magnitudes of intralayer and interlayer Ni(1)–Ni(2) exchange interaction parameters are somewhat lower. It is interesting to note that the Ni(1)–Ni(1) distance for the leading exchange interaction J_1 is very close to that of NiO. At the same time, the values of the corresponding exchange integrals are completely different—about 5 K in $Ni(NO_3)_2$ and about 220 K in NiO [43]. It is due to a different structure of superexchange pathways. In the case of NiO, the superexchange involves one intermediate O^{2-} ion, and the Ni–O–Ni bond angle is equal to 180°, which corresponds to the maximum of the magnetic interaction. On the other hand, the key element of the $Ni(NO_3)_2$ compound (i.e., the NO_3 complex) provides a more distorted pathway between Ni(1) atoms, where Ni(1)–O–N and O–N–O angles are close to 120°.

Based on the calculated exchange interactions, one can estimate the Weiss temperature by using the high-temperature expansion of the magnetic susceptibility $\Theta = \frac{J_0 S(S+1)}{3k_B}$. Here, J_0 is a summary exchange interaction of a given site within the magnetic environment. Despite the fact that the individual magnetic interactions are rather small, the resulting theoretical value of $|\Theta|$ is about $20 \div 40$ K, being significantly larger than found experimentally, which requires additional consideration.

VI. LOW-ENERGY MODEL

As one can see the $Ni(NO_3)_2$ system is described by a rather complex magnetic model where isotropic exchange interactions form a three-dimensional magnetic structure. To reveal the classical magnetic ground state we have performed HF calculations for the model electronic Hamiltonian in Wannier function basis that was defined from the LDA spectrum (Fig. 5) by using the projection procedure [42]. Such a low-energy Hamiltonian reproduces the bands of the e_g symmetry at the Fermi level. Since there is strong nickel-oxygen hybridization, the corresponding Wannier functions contain the Ni $3d$ and O $2p$ contributions.

In the low-energy model, we can readily elucidate the microscopic origin of the exchange interactions J_1, J_2, J_3, and J_4. For these purposes, we first evaluate the averaged transfer integrals $\bar{t}_{ij} = \sqrt{\mathrm{Tr}(\hat{t}_{ij}\hat{t}_{ij})}$, where each $\hat{t}_{ij}$ is the 2×2

matrix in the basis of Wannier orbitals for the e_g bands, and Tr is the trace over orbital indices. This yields the following values: $\hat{t}_1 = 65$ meV, $\hat{t}_2 = 48$ meV, $\hat{t}_3 = 56$ meV, and $\hat{t}_4 = 41$ meV. Thus, the behavior of isotropic exchange interactions can be understood well in the framework of the superexchange theory, where they are related to the form of transfer integrals $J = \frac{\hat{t}_2}{U_{\text{eff}}}$ [44].

The exchange interactions were independently calculated in the low-energy model, taking into account the onsite Coulomb interaction by using the magnetic force theorem (Table I). For the e_g band of $Ni(NO_3)_2$, the onsite Coulomb repulsion and the intra-atomic exchange coupling can be estimated using a combined constrained LDA and random-phase approximation (RPA) techniques, which yield $U = 3.6$ eV and $J_H = 0.8$ eV. The exchange interactions estimated from the low-energy model are two times larger than those obtained from LSDA and LSDA + U. Such an overestimation may be related to the polarization of the oxygen band, which was not explicitly included in the low-energy model [44]. One should also note that the low-energy model is a simplification, which may neglect some contributions to the Js.

VII. MODEL OF THE GROUND STATE

All matrix elements of the relativistic spin-orbit interaction vanish on the basis of the ideal $3z^2$-r^2 and x^2-y^2 e_g orbitals. Therefore, the effects of the spin-orbit interaction on the magnetic structure of $Ni(NO_3)_2$ are expected to be small and caused by the mixing of the t_{2g} and e_g orbitals due to lowering of symmetry and deformation of the perfect NiO_6 octahedra. In such a situation, the main details of the magnetic structure of $Ni(NO_3)_2$, including the ferromagnetic alignment, should be related to the form of isotropic exchange interactions. Then, the central question is how the antiferromagnetic interactions alone can lead to the ferrimagnetic ground state.

Since the exchange interactions of the Ni(1) sublattice are stronger than those between Ni(1) and Ni(2), as the first approximation, one can consider the magnetic structure, which would be formed by the Ni(1) ions, and then the deformation of this structure caused by the Ni(2) ions. Each Ni(1) site interacts with four Ni(1) sites in the plane and four sites between the planes. Importantly, if the central site is Ni(1)-1, it will interact only with sites Ni(1)-2 and Ni(1)-3 (but not with itself), both in and between the planes. Therefore, there is no direct interaction between Ni(1)-1 sites in the neighboring planes, and all of these interactions are mediated by either Ni(1)-2 or Ni(1)-3 sites. Since all of the nearest-neighbor interactions are antiferromagnetic, the effective coupling between Ni(1)-1 sites in the neighboring planes should be ferromagnetic (as the superposition of two antiferromagnetic interactions), while three spins in the same (kagomé) plane satisfy the condition $\mathbf{S}_1 + \mathbf{S}_2 + \mathbf{S}_3 = 0$. This was confirmed by the HF calculations for the low-energy model: after doubling the magnetic cell and enforcing the antiferromagnetic alignment between the planes, the total energy increased by about 0.8 meV/$Ni(NO_3)_2$.

Next, let us consider the interaction between the Ni(1) and Ni(2) sublattices. To be specific, let us consider the umbrella structure, where the Ni(2) spins are presumed to be aligned parallel to the z axis, and the Ni(1) spins form the 120° structure in the xy plane ($\mathbf{S}_1 + \mathbf{S}_2 + \mathbf{S}_3 = 0$), which can be deformed by the interaction with the Ni(2) spin. The deformation causes a canting of the Ni(1) spins out of the xy plane, which can be described by the polar angle θ. Then, the energy gain due to the Ni(1)–Ni(2) interactions is $3\,(J_2 + J_4)\cos\,\theta$, while the energy loss due to the umbrella-type deformation of the Ni(1) sublattice is $6(J_1 + J_3)\cos^2\,\theta$. By minimizing the total energy, we obtain $\cos\,\theta = -\frac{1}{4}\frac{J_2+J_4}{J_1+J_3}$. Using above HF values of J_1–J_4, we find $\theta = 98°$, which is consistent with $\theta = 101°$ obtained in the HF approximation for the low-energy model. For the LSDA and LSDA + U exchange interactions presented in Table I, we obtain 93° and 95°, which are close to the noncollinear HF solution described below.

VIII. CONFIRMATION OF THE NONCOLLINEAR SCENARIO

To verify the proposed microscopic model, we have performed the noncollinear HF calculations [42,45], where each one-electron state is treated as a two-component spinor function. In such calculations, the one-electron part and potential in the HF equations are defined in the general form as nondiagonal in spin variables. The resulting occupation matrix of the system has the same nondiagonal form, which gives us the opportunity to calculate the x, y, and z projection of the atomic magnetic moments.

Figure 7 gives the magnetic ground state obtained from the noncollinear HF calculations. One can see that we obtain the umbrella-type magnetic structure along the z axis described above. Importantly, without spin-orbit coupling, the ground state of the $Ni(NO_3)_2$ is degenerate, and the axis of the umbrella is arbitrary and can be controlled by the external magnetic field.

To compare the magnetic moments obtained in LSDA + U and HF calculations, one should take into account the structure of the Wannier functions used for constructing the low-energy

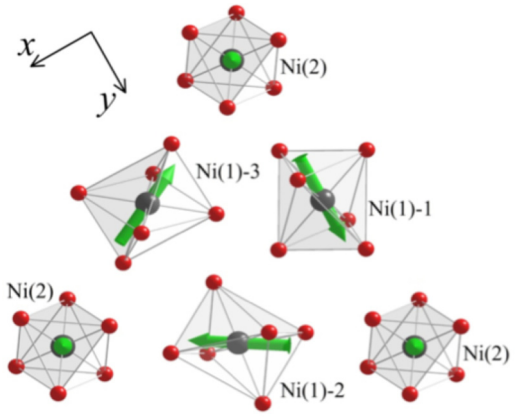

FIG. 7. (Color online) Distributions of the spin magnetic moments in the single xy plane (ab plane), as obtained in the HF calculations for the effective low-energy model. The vectors of magnetic moments (calculated in the Wannier basis) associated with three sites Ni(1) are (0.15, 1.96, −0.38), (1.62, −1.11, −0.38), (−1.77, −0.85, −0.38), and the magnetic moment associated with the site Ni(2) is (0, 0, 2.00). In order to obtain local magnetic moments at the Ni sites themselves, which are reported in our LSDA + U calculations, the above values should be multiplied by the weights of atomic 3d orbitals in the Wannier functions (see discussion in the text).

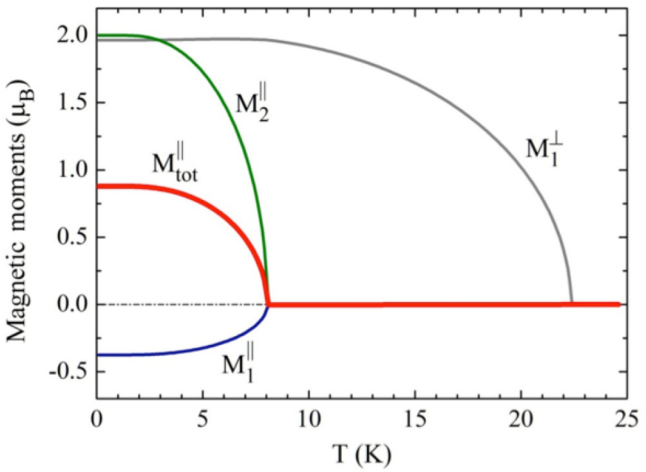

FIG. 8. (Color online) The temperature dependencies of magnetic moments for the noncollinear umbrella structure in the molecular field approximation: components of the magnetic moments of Ni(1) and Ni(2) parallel to the z axis are denoted $M_1^{\parallel}$ and $M_2^{\parallel}$, respectively; the component of the magnetic moment of Ni(1) in the xy plane is denoted $M_1^{\perp}$; and the total ferromagnetic moment is denoted $M_{\rm tot}^{\parallel} = 3M_1^{\parallel} + M_2^{\parallel}$.

model that reproduces the band spectrum of $Ni(NO_3)_2$ near the Fermi level. According to our LDA calculations (Fig. 5), the $3d$-Ni states provide 66% of the electron density; therefore, the effective magnetic moment of the nickel atom from HF calculations can be estimated as $1.33\mu_B$. This value is in agreement with those of LSDA + U, or $1.45\mu_B$. Based on the obtained configuration of the magnetic moments, the $Ni(NO_3)_2$ compound can be classified as a noncollinear ferrimagnet.

To estimate the magnetic transition temperature, we used a molecular field approximation [46] with the exchange interactions calculated within the HF approach. The obtained temperature dependencies for the magnetic moments of the nickel atoms are shown in Fig. 8. In contrast to the original Weiss mean-field approach with a z-oriented effective field, we consider a more complicated situation of the noncollinear magnetic structure. This means that in the case of $Ni(NO_3)_2$, the effective molecular field has x, y, and z projection. As a result, there are two different temperature dependencies for the in-plane and z component of the magnetic moment. The resulting T_c obtained for the total ferromagnetic moment along the z axis is about 8 K, which agrees with the experimental value of 5.5 K. The difference between the calculated spontaneous magnetization of about $0.9\mu_B$ and the measured remanence of about $0.4\mu_B$ could be ascribed to magnetic domain effects. Based on the obtained results, we predict a phase combining an in-plane antiferromagnetic ordering for Ni(1) atoms and magnetic disorder for Ni(2) moments at temperatures between 8 K and 22 K. A negligibly small Weiss temperature Θ of about ± 1 K, defined from high-temperature magnetic susceptibility measurements, tentatively reflects the disorder of Ni(2) magnetic moments.

IX. CONCLUSION

The transition metal nitrate, $Ni(NO_3)_2$, investigated via thermodynamic measurements, XAS, LSDA + U, and HF calculations, appeared to be a low-temperature noncollinear ferrimagnet. Its specific ground state is formed due to the kagomé-type arrangement of one species of nickel ions coupled antiferromagnetically with another species of nickel ions. The frustration of the intraplane exchange interaction in this model is lifted by the 120° arrangement of Ni(1) magnetic moments deformed by an interaction with Ni(2) magnetic moments.

ACKNOWLEDGMENTS

We thank Z. Hu and Y. D. Chuang for discussions on XAS issues. This work was supported in part by the Ministry of Education and Science of the Russian Federation with*in the framework of the* Increase Competitiveness Program of the National University of Science and Technology "MISiS" (Contract No. K2-2014-036), by the Russian Foundation for Basic Research (Grants No. 13-02-00174, 14-02-00111, and 14-02-92002), and by the President of Russia Grants No. MK-7138.2013.2 and MK-5565.2013.2.

[1] P. Sindzingre, G. Misguich, C. Lhuillier, B. Bernu, L. Pierre, Ch. Waldtmann, and H.-U. Everts, Phys. Rev. Lett. **84**, 2953 (2000).
[2] Ch. Waldtmann, H.-U. Everts, B. Bernu, C. Lhuillier, P. Sindzingre, P. Lecheminant, and L. Pierre, Eur. Phys. J. B **2**, 501 (1998).
[3] Y. Okamoto, H. Yoshida, and Z. Hiroi, J. Phys. Soc. Jpn. **78**, 033701 (2009).
[4] K. Hida, J. Phys. Soc. Jpn. **69**, 4003 (2000).
[5] N. Wada, T. Kobayashi, H. Yano, T. Okuno, A. Yamaguchi, and K. Awaga, J. Phys. Soc. Jpn. **66**, 961 (1997).
[6] H. Kato, M. Kato, K. Yoshimura, and K. Kosuge, J. Phys. Soc. Jpn. **70**, 1404 (2001).
[7] S. Hara, H. Sato, and Y. Narumi, J. Phys. Soc. Jpn. **81**, 073707 (2012).
[8] W. Miiller, M. Christensen, A. Khan, N. Sharma, R. B. Macquart, M. Avdeev, G. J. McIntyre, R. O. Piltz, and C. D. Ling, Chem. Mater. **23**, 1315 (2001).
[9] M. Kato, Physica B **329–333**, 1042 (2003).
[10] J. Behera and C. N. Rao, J. Am. Chem. Soc. **128**, 9334 (2006).
[11] D. E. Freedman, R. Chisnell, T. M. McQueen, Y. S. Lee, C. Payen, and D. G. Nocera, Chem. Commun. **48**, 64 (2012).
[12] G. Lawes, M. Kenzelmann, N. Rogado, K. H. Kim, G. A. Jorge, R. J. Cava, A. Aharony, O. Entin-Wohlman, A. B. Harris, T. Yildirim, Q. Z. Huang, S. Park, C. Broholm, and A. P. Ramirez, Phys. Rev. Lett. **93**, 247201 (2004).
[13] M. Kenzelmann, A. B. Harris, A. Aharony, O. Entin-Wohlman, T. Yildirim, Q. Huang, S. Park, G. Lawes, C. Broholm, N. Rogado, R. J. Cava, K. H. Kim, G. Jorge, and A. P. Ramirez, Phys. Rev. B **74**, 014429 (2006).

[14] J. Wang, M. Tokunaga, Z. Z. He, J. I. Yamaura, A. Matsuo, and K. Kindo, Phys. Rev. B **84**, 220407(R) (2011).
[15] F. Pollmann, P. Fulde, and K. Shtengel, Phys. Rev. Lett. **100**, 136404 (2008).
[16] Y. Tomita, J. Phys. Soc. Jpn. **78**, 114004 (2009).
[17] K. Damle and T. Senthil, Phys. Rev. Lett. **97**, 067202 (2006).
[18] S. Tanaka and S. Miyashita, J. Phys. Soc. Jpn. **76**, 103001 (2007).
[19] L. Berger, S. A. Friedberg, and J. T. Schriempf, Phys. Rev. **132**, 1057 (1963).
[20] R. Zibaseresht and R. M. Hartshorn, Acta Cryst. E **62**, i19 (2006).
[21] O. S. Volkova, I. V. Morozov, E. N. Lapsheva, V. V. Shutov, A. N. Vasiliev, R. Klingeler, and B. Büchner, JETP Lett. **89**, 88 (2009).
[22] L. Berger and S. A. Friedberg, Phys. Rev. **136**, A158 (1964).
[23] C. C. Addison and B. M. Gatehouse, J. Chem. Soc. 613 (1960).
[24] C. D. Garner, R. W. Hawksworth, I. H. Hillier, A. A. MacDowell, and M. F. Guest, J. Am. Chem. Soc. **102**, 4325 (1980).
[25] G. Giester, C. L. Lengauer, M. Wildner, and J. Zemann, Z. Kristallogr. **223**, 408 (2008).
[26] G. A. Tikhomirov, K. O. Znamenkov, E. Kemnitz, and S. I. Troyanov, Z. Anorg. Allg Chem. **628**, 269 (2002).
[27] G. A. Bain and J. F. Berry, J. Chem. Educ. **85**, 532 (2008).
[28] Y. Yamaguchi and N. Sakamoto, J. Phys. Soc. Jpn. **27**, 1444 (1969).
[29] M. W. Haverkort, Ph.D. thesis, Koeln University, 2005.
[30] I. Preda, M. Abbate, A. Gutierrez, S. Palacin, A. Vollmer, and L. Soriano, ELSPEC, **156–158**, 111 (2007).
[31] J.-S. Kang, H. J. Lee, D. H. Kim, S. Kolesnik, B. Dabrowski, K. Świerczek, J. Lee, B. Kim, and B. I. Min, Phys. Rev. B **80**, 045115 (2009).
[32] A. Tanaka and T. Jo, J. Phys. Soc. Jpn. **63**, 2788 (1994).
[33] M. W. Haverkort, S. I. Csiszar, Z. Hu, S. Altieri, A. Tanaka, H. H. Hsieh, H.-J. Lin, C. T. Chen, T. Hibma, and L. H. Tjeng, Phys. Rev. B **69**, 020408 (2004).
[34] L. A. Wray, W. Yang, H. Eisaki, Z. Hussain, and Y.-D. Chuang, Phys. Rev. B **86**, 195130 (2012).
[35] W. Mi, H. Yang, Y. Cheng, and H. Bai, Sol. St. Comm. **152**, 1108 (2012).
[36] E. Konysheva, E. Suard, and J. T. S. Irvine, Chem. Mater. **21**, 5307 (2009).
[37] A. I. Lichtenstein, M. I. Katsnelson, V. P. Antropov, and V. A. Gubanov, J. Magn. Magn. Mater. **67**, 65 (1987).
[38] V. V. Mazurenko and V. I. Anisimov, Phys. Rev. B **71**, 184434 (2005).
[39] O. K. Andersen, Phys. Rev. B **12**, 3060 (1975).
[40] O. K. Andersen and O. Jepsen, Phys. Rev. Lett. **53**, 2571 (1984).
[41] V. I. Anisimov, J. Zaanen, and O. K. Andersen, Phys. Rev. B **44**, 943 (1991).
[42] I. V. Solovyev, J. Phys.: Condens. Matter **20**, 293201 (2008).
[43] M. T. Hutchings and E. J. Samuelsen, Phys. Rev. B **6**, 3447 (1972).
[44] In the Hubbard model, U_{eff} is given by $U_{\text{eff}} = U + J_{\text{H}}$ where U and J_{H} are the onsite Coulomb repulsion and the intra-atomic exchange coupling, respectively.
[45] I. V. Solovyev, Phys. Rev. B **74**, 054412 (2006).
[46] I. V. Solovyev, New Journal of Physics **11**, 093003 (2009).